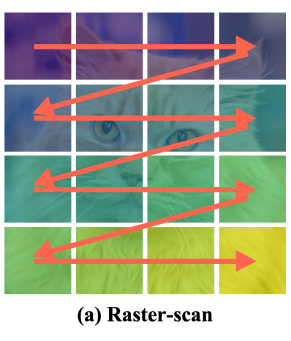
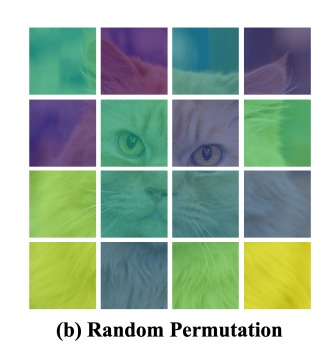
# **Spanning Tree Autoregressive Visual Generation**

Sangkyu Lee<sup>1,2\*</sup> Changho Lee<sup>3</sup> Janghoon Han<sup>3</sup> Hosung Song<sup>3</sup>
Tackgeun You<sup>2</sup> Hwasup Lim<sup>2</sup> Stanley Jungkyu Choi<sup>3</sup> Honglak Lee<sup>3,4</sup> Youngjae Yu<sup>5</sup>
Yonsei University<sup>1</sup> KIST<sup>2</sup> LG AI Research<sup>3</sup>
University of Michigan, Ann Arbor<sup>4</sup> Seoul National University<sup>5</sup>





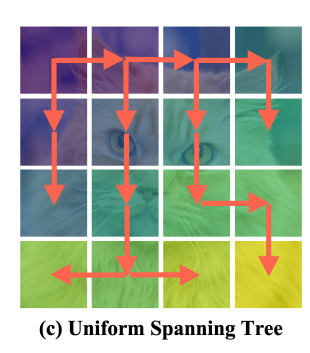


Figure 1. Comparison of sequence orders in AR visual generation. (a) Conventional AR models follow a fixed raster-scan order, which limits the capability to change the sequence order at inference. (b) AR models trained under random permutation have flexibility on inference sequence order, but random permutation does not reflect prior knowledge, such as center bias and locality. (c) The proposed method, STAR, adopts the traversal order of the uniform spanning tree so that it structurally maintains prior knowledge and flexibility.

#### **Abstract**

We present Spanning Tree Autoregressive (STAR) modeling, which can incorporate prior knowledge of images, such as center bias and locality, to maintain sampling performance while also providing sufficiently flexible sequence orders to accommodate image editing at inference. Approaches that expose randomly permuted sequence orders to conventional autoregressive (AR) models in visual generation for bidirectional context either suffer from a decline in performance or compromise the flexibility in sequence order choice at inference. Instead, STAR utilizes traversal orders of uniform spanning trees sampled in a lattice defined by the positions of image patches. Traversal orders are obtained through breadth-first search, allowing us to efficiently construct a spanning tree whose traversal order ensures that the connected partial observation of the image appears as a prefix in the sequence through rejection sampling. Through the tailored yet structured randomized strategy compared to random permutation, STAR preserves the capability of postfix completion while maintaining sampling performance without any significant changes to the model architecture widely adopted in the language AR modeling. \(^1\)

#### 1. Introduction

The scalability of the *next-token prediction* pretraining scheme of autoregressive (AR) models built on a Decoderonly Transformer architecture [14, 19, 29] has yielded remarkable results in language generation, such as large language models [29, 37]. Meanwhile, the success of the Decoder-only Transformer has led to the transition of AR modeling for visual generation [38, 39] to the next-patch prediction scheme, which typically predicts the next token representing a single patch by the predefined raster-scan order. Similar to the language generation, AR modeling of visual generation through the next-token prediction scheme also exhibits efficient scaling behavior [11, 20, 25], highlighting the competitive advantage of AR visual modeling compared to other methods for visual generation [1, 5, 17, 23, 28]. Furthermore, the architecture that can seamlessly integrate with language generation serves as a cornerstone of early-fusion multimodal models [35] supporting native generation capabilities in both language and image.

However, conventional AR visual modeling restricts the 2D nature of images only to *unidirectional* contexts in a specific direction defined by the fixed sequence order. To address the unidirectional problem of the conventional AR models in visual generation, recent approaches [23, 26, 44] adopt the *random permutation* [6, 27, 42] to shuffle the se-

<sup>\*</sup>Work mainly done during internship at LG AI Research.

<sup>&</sup>lt;sup>1</sup>The code is available at github.com/oddqueue/star.

quence order and provide the position of next patches to be predicted as additional conditions to expose the image as *bidirectional* contexts to AR models by diverse sequence order during training. Nevertheless, AR models trained with randomized sequence orders tend to suffer from degraded sampling performance compared to conventional AR models that follow a fixed raster-scan order, despite having the capability of inference under arbitrary sequence orders.

In this paper, we present Spanning Tree Autoregressive (STAR) modeling, a structured order randomization strategy based on the uniform spanning tree for AR visual generation models by revisiting the characteristic of rasterscan order and random permutation, as shown in Figure 1. Training solely in raster-scan order forces the choice of sequence order at inference but guarantees continuity in the 2D lattice, between the tokens that are in the prefix of the sequence and the token to be predicted, and starts from the corner where salient objects are unlikely to appear. On the other hand, random permutation does not guarantee this continuity, but it does guarantee diverse sequence orders due to randomness. This is the motivation of our approach, which traverses a uniform spanning tree, as a representative example of satisfying the advantages of both, reflecting prior knowledge of images, such as center bias [3, 33] and locality [2, 18], yet preserving randomness for flexibility.

Specifically, we consider the traversal order obtained by breadth-first search (BFS) of a uniform sampling tree, with a random corner as the root node, as the sequence order. By choosing the BFS traversal order, we can efficiently sample the spanning tree that can handle the image editing task as a postfix completion task through rejection sampling at inference, when the partial observation of the image is connected, which was not available to the conventional rasterorder AR visual generation model. Furthermore, STAR requires minimal changes to the conventional Decoder-only Causal AR Transformer, only additional positional embeddings that perform conditioning for the next token position to be predicted [27, 44] are required as random permutation strategies, but outperforms their sampling performance.

Our contribution to the AR visual generation can be summarized as threefold: (1) We propose STAR, an order randomization strategy for AR visual generation that structurally reflects prior knowledge about the image while ensuring flexibility in the choice of sequence order at inference for downstream tasks, based on the uniform sampling tree. (2) We show that the BFS traversal order of uniform spanning trees is sufficient to enjoy the benefit of random permutation, offering the opportunity to be exposed to bidirectional context, without increasing the training complexity. (3) We offer a new building block for future work of AR visual generation in image editing, which is challenging in conventional AR visual models, and can be adopted through minimal changes without sacrificing performance.

## 2. Related Works

Unidirectional AR Visual Generation Decoder-only Transformer proposed by GPT-2 [29], which adopts the causal attention mask, has become the de facto standard architecture for AR language modeling [4, 37] due to its advantageous feature of scaling behavior [14, 19]. The success of the Decoder-only Transformer, often represented by next-token prediction, has enriched the research direction of image generation based on AR modeling [38, 39] to next-token prediction. A sequence of research for nexttoken prediction for image generation [12, 32, 43] achieves AR visual modeling by training to predict patch representations of images, typically arranged in a predefined, unidirectional order, such as raster-scan order. Sharing the architecture across data modalities facilitates expansion into earlyfusion multimodal models [35], but unidirectional modeling of images imposes limitations on image editing, due to the 2D structure of images. Inspired by this aspect, we aim to enable flexible downstream task capabilities of AR visual generation without significant changes to the architecture.

Bidirectional Context for Visual Generation A line of research has been conducted to accommodate the bidirectional context for visual generation. One research direction is introducing bidirectional transformers for masked token prediction [5], diffusion models [1, 17, 28], or mimicking AR models with a diffusion loss [23], but often shows less efficiency than the causal AR model in scaling behavior [20, 25]. Another approach decouples spatial prediction of images in AR visual modeling and introduces a dedicated transformer architecture [22, 36], but this limits the extension to early-fusion multimodal models. The other approach exposes bidirectional contexts to AR models by applying random permutation to the sequence order [6] and providing the conditions for next token position through position instruction tokens [26], additional positional embeddings [27, 44], or multi-stream attention mechanisms [23, 42], but commonly trade either sampling performance or flexibility in sequence order at inference. As an extension of the last approach, we introduce a method that enhances the trade-off between performance and flexibility while preserving the causal AR Transformer architecture.

#### 3. Method

In this section, we describe our approach, **Spanning Tree Autoregressive (STAR)** modeling, which generates visual tokens in an autoregressive fashion following the traversal order of the spanning tree to impose structurally randomized sequence orders for preserving sampling performance, yet flexible choice of sampling order, as shown in Figure 2.

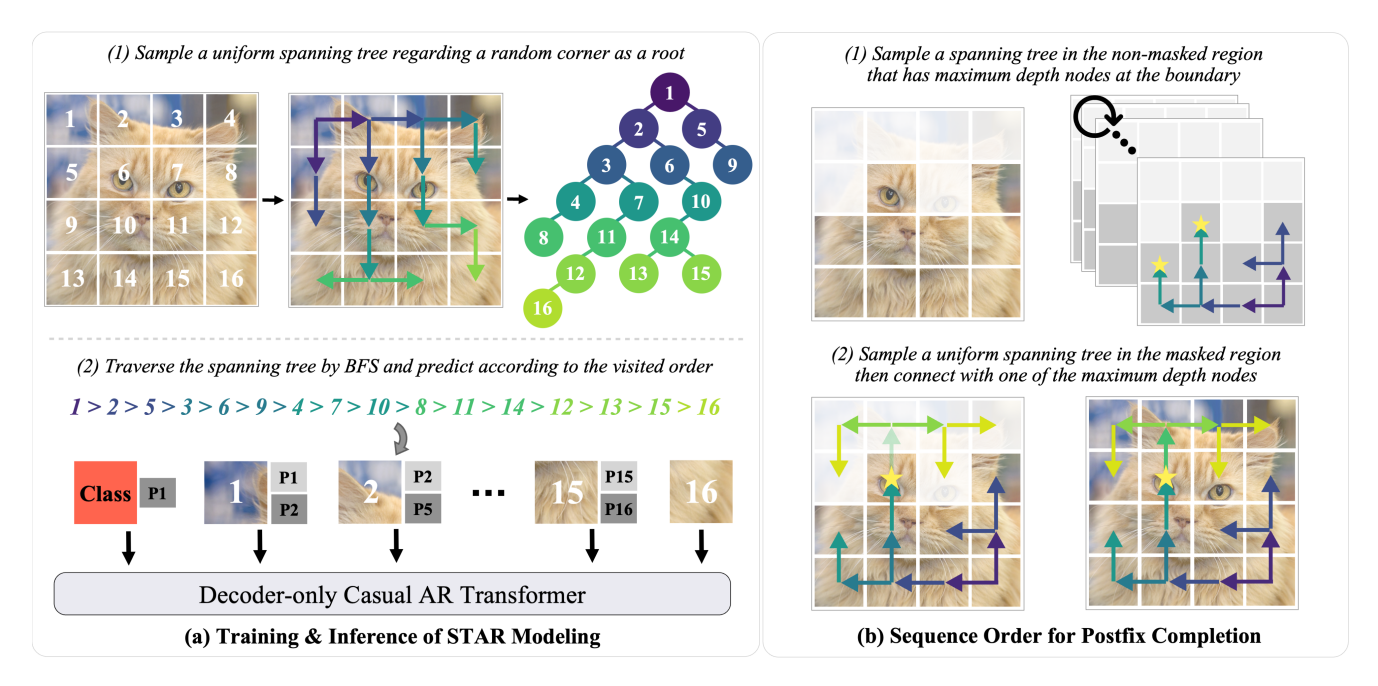


Figure 2. Overview of the proposed STAR modeling. (a) We perform training and inference according to the sequence order obtained by traversing the uniform sampling tree from the corner using BFS, by additionally feeding the positional embedding for the next token position to the model. (b) We perform rejection sampling to sample a spanning tree with a maximum depth occurring at the boundary of the non-masked region, allowing postfix completion when partial observations of the image are provided for image editing.

#### 3.1. From Fixed To Randomized Orders

As a generative model for visual generation, AR models approximate the marginal distribution of image x by factorizing into multiple conditional distributions and estimate it through maximum likelihood estimation. Here, the conventional approach regards the image as a collection of token representation of patch  $\{x_{i,j}\}$  whose size is  $h \times w$  and linearizes the 2D position of the tokens to the 1D sequence order  $\tau := (\tau_1, \cdots \tau_N)$  where  $N = h \times w$ . Formally, AR models  $p_\theta$  in visual generation are trained as follows,

$$\underset{\theta}{\operatorname{argmax}} \ p_{\theta}(x) = \prod_{i=1}^{N} p_{\theta}(x_{\tau_i} | x_{\tau_1}, x_{\tau_2}, \dots x_{\tau_{i-1}}). \tag{1}$$

The sequence order  $\tau$  is a distinctive feature of AR modeling for visual generation compared to natural language generation. Unlike natural languages, which exhibit a relatively straightforward left-to-right sequence order, it is challenging to impose an adequate sequence order on images due to their inherent structure. The empirically practical approach is to adopt a predefined sequence order, specifically raster-scan order, as it often demonstrates better performance compared to other sequence orders [11, 12, 44].

However, adopting a single, fixed sequence order presents a problem in that it exposes the image to the AR model only in a unidirectional sequence order and prevents conditioning on token representations at positions that do not appear as a prefix in the predefined sequence order, un-

like bidirectional modeling approaches. It results in a structural limitation, making it challenging to perform downstream tasks such as image editing, which requires the capability of completing the postfix for partial observation when an image is masked and given as a prefix of a sequence.

In this context, some approaches sample sequence order from random permutations  $\sigma(N)$  during training, rather than fixing the sequence order to a single predefined order [6, 23, 26, 44]. The common goal is to enable AR models to be trained on bidirectional contexts in *expectation*, by uniformly sampling the random sequence order,

$$\underset{\theta}{\operatorname{argmax}} \ p_{\theta}(x) = \mathbb{E}_{\tau \sim \sigma(N)} \Big[ \prod_{i=1}^{N} p_{\theta}(x_{\tau_i} | x_{\tau_{< i}}) \Big]. \tag{2}$$

AR models trained with randomized sequence orders gain an additional advantage; predictions on arbitrary sequence orders at inference become possible, which is beneficial for specific downstream tasks such as image editing. However, previous approaches that adopt random permutation generally suffer from degraded sampling performance compared to the fixed raster-scan order, despite its expandability to downstream tasks. It suggests a motivation for a tailored randomized order that enables bidirectional context to AR models, while leveraging the structural advantages of predefined sequence order in visual generation.

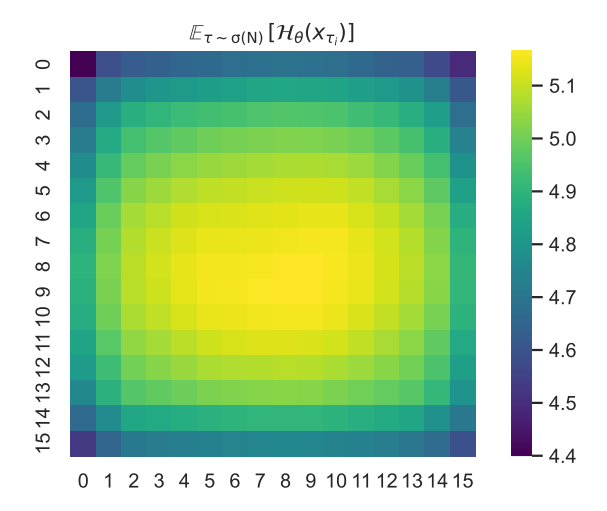


Figure 3. Prediction entropy of tokens according to token position from the model trained with randomly permuted sequence orders. Higher token entropy in central regions indicates greater token diversity compared to corner areas. The evidence that such differences exist suggests a potential hierarchical structure across the position, affecting the differences in the difficulty of prediction.

## 3.2. Uniform Spanning Tree for AR Modeling

Random permutations provide a natural bidirectional modeling property on AR models, but the factorial growth (N!) of possible sequence orders makes it challenging to discover advantageous sequence orders, such as raster-scan order. This limitation highlights the necessity to narrow the sample space of sequence order used for training bidirectional contexts by identifying common properties among specific sequence orders that empirically perform well. A plausible conjecture is that the advantage of predefined sequences derives from *prior knowledge* of the image, such as center bias [3, 33] or correlation between adjacent pixels [2, 18].

To verify whether similar phenomena persist in token representations of images, we measure prediction entropy  $\mathcal{H}_{\theta}(x_{\tau_i})$  and conditional prediction entropy  $\mathcal{H}_{\theta}(x_{\tau_i} \mid x_{\tau_{<i}})$  of AR model trained with random permutation using ImageNet-1k [8] by sampling 100 random permutation for each validation image. Figure 3 and Figure 4 demonstrate that prior knowledge about the image is still maintained even in token representations; AR models for visual generation show difficulty in predicting token positions moving away from the already predicted tokens or moving towards the central region. In particular, the fact that conditional prediction entropy increases rapidly when the distance from adjacent tokens slightly increases suggests that the partial observation of the image cannot be utilized as a meaningful context if it is not connected to the token to be predicted.

In this context, we propose an approach that utilizes the *uniform spanning tree* on a lattice corresponding to the position relationships of token representations of an image to

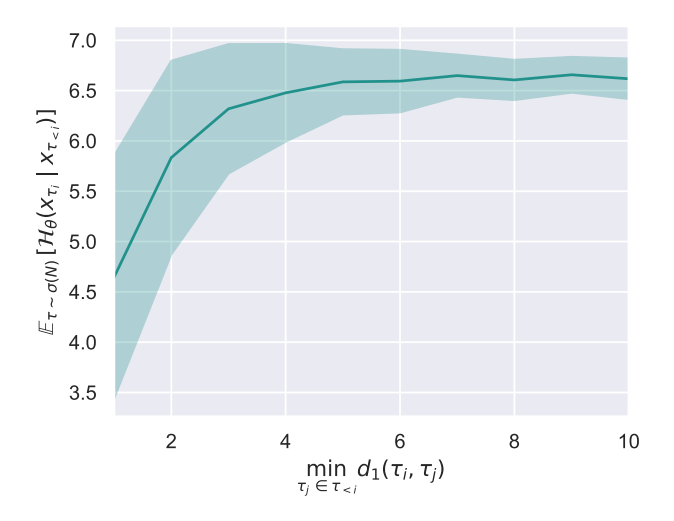


Figure 4. Conditional prediction entropy according to the minimum Manhattan distance from the prefix token positions. Tokens located at closer distances tend to exhibit lower entropy, whereas those farther away show higher entropy. This suggests that the locality structure of images is partially preserved at the tokens, implying that adjacent tokens should be prioritized in prediction.

structurally reflect prior knowledge about the image in the order randomization strategy. Formally, we regard the token position (i,j) as a vertex v and each vertex is connected by an edge as a regular taxicab lattice. From the lattice  $G \coloneqq (V,E)$ , we uniformly sample a spanning tree  $T \sim \mathcal{T}(G,r)$  by regarding the random corner vertex as a root node r. Naturally, the sequence order of traversing the spanning tree from the corners will move towards the central region while predicting adjacent tokens to the prefix.

Furthermore, the spanning tree enables the exposure of bidirectional context to the AR model while preventing it from being exposed to unnecessary sequence orders for inference. It is known that the number of spanning trees asymptotically follows  $\exp(N\cdot z_G)$  as  $N\to\infty$  where  $z_G$  is a constant defined by the lattice type,  $z_G\approx 1.166$  for our regular taxicab lattice [31]. Therefore, the number of spanning trees exhibits exponential growth with N, a distinctly smaller sample space compared to the N! sample space of random permutations. Still, the uniform spanning tree can be efficiently sampled based on the loop-erased random walk, also known as Wilson's algorithm [41].

### 3.3. Traversal Order for Postfix Completion

Traversing a uniform spanning tree enables the construction of a bidirectional context while leveraging prior knowledge about the image; however, it does not directly guarantee compatibility of the downstream task, where partial observations of the masked image are available at inference, such as in image editing. Under the assumption that the partial observation of an image is connected and the masked do not

cover every corner of the lattice G, it requires to be easy to sample a spanning tree in which the partial observations of image tokens appear sequentially as a prefix and the masked region appears as a postfix in the sequence order, to regard the image editing as a postfix completion task of the given sequence. Therefore, we need to choose an adequate traversal strategy that can easily sample a spanning tree satisfying the requirement for postfix completion at inference time.

Representative approaches for traversing a tree structure include the depth-first search (DFS) and breadth-first search (BFS) algorithms. However, under a fixed tie-breaking rule, BFS has an advantage over DFS in the acceptance ratio of rejection sampling when sampling a spanning tree for post-fix completion. Formally, when the masked token region of the given image is denoted as  $M := (V_M, E_M) \subset G$ , the following condition must be satisfied for the spanning tree T for G to be able to perform postfix completion,

$$\operatorname{depth}_{T}(v_{M}) > \operatorname{depth}_{T}(v) \ \forall v \in V \setminus V_{M}, v_{m} \in V_{M}.$$
 (3)

That is, the depth of vertices in the spanning tree of the vertex excluding the masked region M must be shallower than that of all vertices belonging to M. This condition is equivalent to the restriction of the spanning tree  $T|_{V\setminus V_M}$  having maximum depth at boundary B, which is the collection of vertices in  $V\setminus V_M$  adjacent to M. Therefore, it is sufficient as long as one of the vertices with the maximum depth is adjacent to M when we sample a spanning tree using vertices in  $V\setminus V_M$ , even if M is not adjacent to the last appearing vertex in the BFS traversal order of itself. However, if we adopt DFS for traversal, a more strict condition must be satisfied: the exactly one vertex visited last in the DFS traversal order of the tree spanning on  $V\setminus V_M$  must be adjacent to M, under the fixed tie-breaking rule.

Therefore, we train the AR model  $p_{\theta}$  by maximum likelihood estimation using the BFS traversal order of the uniform spanning tree, by providing additional positional embedding for the next token position [27, 44]. Additionally, we regard all corners in the lattice as candidates for root R and uniformly sample a random root R as follows,

$$\underset{\theta}{\operatorname{argmax}} \ \mathbb{E}_{r \sim R, \ \tau \sim \operatorname{BFS}(\mathcal{T}(G, r))} \Big[ \prod_{i=1}^{N} p_{\theta}(x_{\tau_{i}} | x_{\tau_{< i}}) \Big]. \tag{4}$$

When partial observation of the image is not provided at inference time, we use the BFS traversal order of the uniform spanning tree, with one random vertex belonging to the corner serving as the root, as the sequence order, similar to training time. If partial observation is given, we first obtain the spanning tree in the non-masked region that enables postfix completion through rejection sampling, while regarding the farthest corner on average from the boundary B in Manhattan distance as the root node to increase the acceptance ratio. We select one random vertex in the masked

## Algorithm 1 Sequence Order for Postfix Completion

```
Require: lattice G := (V, E), mask M := (V_M, E_M)
Ensure: M \subset G, corner(G) \not\subset M, G \setminus M is connected
  1: # find boundary of unmasked region
  2: G' \leftarrow (V \setminus V_M, \{(u, v) \in E \mid u, v \notin V_M\})
  3: B \leftarrow \{v \in V \setminus V_M \mid \exists u \in V_M \text{ s.t. } (u, v) \in E\}
  4: # find the farthest root node
  5: R_{G'} \leftarrow \{v \in \operatorname{corner}(G) \mid v \notin M\}
 6: r_{G'} \leftarrow \operatorname{argmax}_{r \in R_{G'}} \frac{1}{|B|} \sum_{v \in B} d_1(v,r)
7: # spanning tree for unmasked region
        T_{G'} \sim \mathcal{T}(G', r_{G'})
        d_{\max} \leftarrow \max_{v \in T_{G'}} \operatorname{depth}_{T_{G'}}(v, r_{G'})
        V_{G_{\max}'} \leftarrow \{v \in T_{G'} \mid \operatorname{depth}_{T_{G'}}(v, r_{G'}) = d_{\max}\}
12: until B \cap V_{G'_{\max}} \neq \emptyset
13: # spanning tree for masked region
14: R_M \leftarrow \{v \in V_M \mid \exists u \in V_{G'_{max}} \text{ s.t. } (u, v) \in E\}
15: r_M \sim R_M
16: T_M \sim \mathcal{T}(M, r_M)
17: # construct the sequence order
18: \tau_{G'} \leftarrow \mathrm{BFS}(T_{G'})
19: \tau_M \leftarrow \text{BFS}(T_M)
20: \tau \leftarrow [\tau_{G'}, \tau_M]
21: return sequence order \tau
```

region adjacent to the maximum depth nodes in B and treat it as the new root for the spanning tree of the masked region. Finally, we complete the spanning tree by uniformly sampling a spanning tree in the masked region from the selected root node, and we perform a BFS traversal for the entire spanning tree to obtain the final sequence order. Algorithm 1 summarizes the entire process of sampling sequence order for postfix completion at inference.

#### 4. Experiments

## 4.1. Implementation Details

Dataset and Model Architecture We assess the feasibility of STAR by class-conditional generative models for  $256 \times 256$  resolution image using ImageNet-1k [8] with minimal changes to the conventional Decoder-only AR Transformer, following the configurations proposed by RAR [44]. We utilize MaskGIT-VQGAN [5] as the tokenizer model, trained on ImageNet-1k at a resolution of  $256 \times 256$ , to obtain discretized patch representation sequences, similar to prior works [12, 44]. This tokenizer is based on a CNN-based VQ autoencoder, with a codebook size of 1024 and a downsampling rate of 16; therefore, we represent a single  $256 \times 256$  sized image as a collection of 256 tokens. We utilize an architecture based on the ViT [10] model for AR models, along with additional features such as a standard causal AR attention mask, QK LayerNorm [7].

Table 1. Comparison of class-conditional image generation models on ImageNet-1k at  $256 \times 256$ . We report Fréchet Inception Distance (FID), Inception Score (IS), Precision (Prec.), and Recall (Rec.).  $\downarrow$  or  $\uparrow$  indicates that lower or higher values are better on the given metric.

Token Type	Model Type	Model	# Params	$\textbf{FID}(\downarrow)$	$\mathbf{IS}(\uparrow)$	$\mathbf{Prec.}(\uparrow)$	$\mathbf{Rec.}(\uparrow)$
	Diffusion	UViT-L/2 [1]	287M	3.40	219.9	0.83	0.52
Continuous		UViT-XL/2 [1]	501M	2.29	263.9	0.82	0.57
		DiT-L/2 [28]	458M	5.02	167.2	0.75	0.57
		DiT-XL/2 [28]	675M	2.27	278.2	0.83	0.57
	Bidirectional AR	MAR-B [24]	208M	2.31	281.7	0.82	0.57
		MAR-L [24]	479M	1.78	296.0	0.81	0.60
		MAR-H [24]	943M	1.55	303.7	0.81	0.62
	Raster-scan Causal AR	LlamaGen-L [32]	343M	3.80	248.3	0.83	0.51
		LlamaGen-XL [32]	804M	3.39	227.1	0.81	0.54
		LlamaGen-XXL [32]	1.4B	3.09	253.6	0.83	0.53
		LlamaGen-3B [32]	3.0B	3.05	222.3	0.80	0.58
		RAR-B [44]	261M	1.95	290.5	0.82	0.58
		RAR-L [44]	461M	1.70	299.5	0.81	0.60
Discrete		RAR-XL [44]	955M	1.50	306.9	0.80	0.62
		RAR-XXL [44]	1.5B	1.48	326.0	0.80	0.63
	Block-wise Causal AR	VAR-d16 [36]	310M	3.30	274.4	0.84	0.51
		VAR-d20 [36]	600M	2.57	302.6	0.83	0.56
		VAR-d24 [36]	1.0B	2.09	312.9	0.82	0.59
		VAR-d30 [36]	2.0B	1.92	323.1	0.82	0.59
	Randomized Causal AR	RandAR-L [26]	343M	2.55	288.8	0.81	0.58
		RandAR-XL [26]	775M	2.25	314.2	0.80	0.60
		RandAR-XXL [26]	1.4B	2.15	322.0	0.79	0.62
		STAR-B	261M	2.24	295.3	0.82	0.57
		STAR-L	461M	1.98	322.0	0.82	0.58
		STAR-XL	955M	1.65	333.2	0.80	0.62
		STAR-XXL	1.5B	1.55	338.8	0.81	0.62
MA MARKET SALES							4.0%



Figure 5. Examples of sampled results from STAR-XXL in the class-conditional image generation on ImageNet-1k at  $256 \times 256$ .

The class conditioning is provided through the first token in the sequence and adaLN [28]. We train additional learnable positional embeddings for the positions of the next token to be predicted [27, 44]. We scale the model into four configurations, STAR-B, STAR-L, STAR-XL, and STAR-XXL.

**Training and Evaluation** We tokenize each image by applying a ten-crop transformation [34, 44] and train for 250k steps with a batch size of 2048 ( $\sim$  400 epochs) for all configurations. We use AdamW with a cosine learning rate, with a peak learning rate of 4e-4 and a linear warmup for 0.25 total training steps. The uniform spanning tree is sampled through Wilson's algorithm [41], and a fixed tiebreaking rule, which first visits the index preceding it in

raster order, is applied to children with the same parent during BFS traversal. The dropout out of class conditioning is performed with a probability of 0.1 for classifier-free guidance [16], and power-cosine scheduling [13, 40], without the top-p or top-k sampling, is adopted at inference. For evaluating the class-conditional image generation, we follow the evaluation protocol of ADM [9] and report the Fréchet Inception Distance (FID) [15], Inception Score (IS) [30], Precision, and Recall [21]. Additionally, we extend this evaluation protocol to the image inpainting setting for a quantitative evaluation of image editing capabilities. After tokenizing the validation images in ImageNet-1k, we drop a random connected subset of tokens whose size is a given ratio of the entire number of tokens, and re-

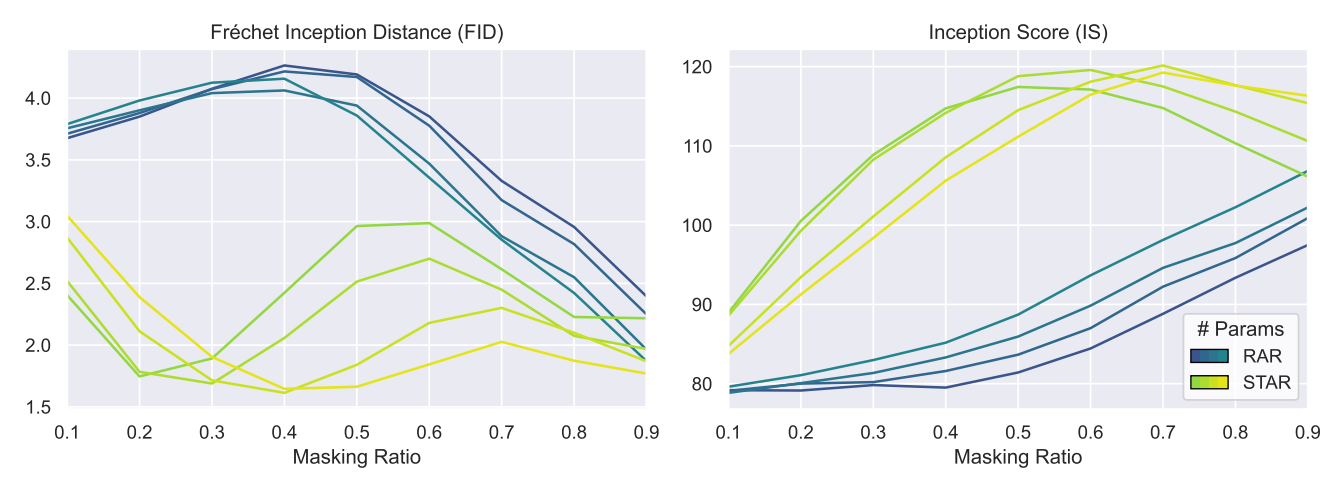


Figure 6. Quantitative comparison of RAR [44] and STAR on the inpainting task with varying masking ratio from 0.1 to 0.9.



Figure 7. Qualitative comparison on the inpainting task, demonstrating insufficient results of RAR-XXL [44] compared to STAR-XXL.

gard the remaining tokens as a partial observation of each image provided for image inpainting. Further implementation details are described in the supplementary material.

#### 4.2. Main Results

Class-conditional Image Generation In Table 1, we compare STAR with state-of-the-art class-conditional image generation models trained on ImageNet-1k at  $256 \times 256$ . We observe that our simple modification, which introduces sequence order randomization via the traversal order of the uniform spanning tree to conventional AR models, such as LlamaGen [32], can achieve performance that is sufficiently comparable with state-of-the-art models without increasing the training complexity, such as the order annealing strategy of RAR [44] that requires additional hyperparameter search and architectural changes of VAR [36] that requires a block-wise causal attention mask and tailored tokenizer. In addition, STAR also outperforms RandAR [26], which adopts random permutation of sequence orders during training, demonstrating the effectiveness of spanning trees compared to random permutation in randomized order training. Considering that MAR [23] utilizes random permutation,

along with diffusion loss and a continuous VAE tokenizer, the notable performance of STAR in the AR Transformer, trained by cross-entropy loss with a discrete VQ tokenizer, shows a promising direction of future extension. Figure 5 illustrates sampled results from STAR-XXL, and more examples are included in the supplementary material.

Comparison of Inpainting Capability In Figure 6, we evaluate the image inpainting capabilities of STAR according to the change of masking ratio, compared with RAR [44], to verify whether image editing capability can be achieved even with a fixed sequence order if exposed to a bidirectional context during training. We provide the partial observation of the image as a prefix for STAR and through teacher forcing without sampling from the model for RAR. We observe that the FID in the range of 0.4 to 0.6, where approximately half of the image can be considered conditioned in the results of STAR, is significantly improved by scaling the model size. We speculate that the lack of diversity to sufficiently cover the validation data distribution leads to a poor recovery of the plausible sample from the ambiguous but still meaningful partial observations, based

Table 2. Ablation study on the order randomization strategy. "Start" and "End" denote the sequence order at the start or end, and perform order annealing at 0.5 to 0.75 of the total steps [44]. We report the average score of mask ratios from 0.1 to 0.9 on the inpainting task.

Training		Inference	Generation			Inpainting				
Start	End		$\overline{\mathbf{FID}(\downarrow)}$	IS(↑)	Prec.(↑)	Rec.(†)	$\overline{\text{FID}}(\downarrow)$	IS(↑)	Prec.(↑)	Rec.(†)
Raster-scan	Raster-scan	Raster-scan	2.04	266.5	0.80	0.59	3.91	82.7	0.75	0.60
Random	Random	Random	3.57	291.4	0.78	0.57	2.57	108.7	0.82	0.56
Random	Random	Spanning Tree	3.58	234.9	0.76	0.60	2.43	105.8	0.83	0.56
Random	Spanning Tree	Spanning Tree	2.31	285.2	0.81	0.57	2.35	107.9	0.83	0.56
Spanning Tree	Spanning Tree	Spanning Tree	2.24	295.3	0.82	0.57	2.39	108.8	0.83	0.56

Table 3. Ablation study on the sample efficiency according to the traversal strategy of the spanning tree for postfix completion.

	# Average Trial for Accept (Failure Ratio)					
Masking Ratio	D	FS	BFS			
	Random Farthest		Random	n Farthest		
0.1	60.45 (50.1)	89.37 (82.3)	5.59 (0.0)	4.41 (0.0)		
0.2	52.09 (41.8)	80.25 (70.0)	3.56 (0.0)	3.03 (0.0)		
0.3	44.63 (33.0)	70.45 (57.9)	2.76 (0.0)	2.50 (0.0)		
0.4	36.87 (24.9)	53.70 (40.4)	2.11 (0.0)	1.95 (0.0)		
0.5	29.31 (17.4)	23.33 (12.3)	1.60 (0.0)	1.57 (0.0)		
0.6	23.28 (11.6)	19.7 (9.8)	1.49 (0.0)	1.51 (0.0)		
0.7	13.62 (3.0)	14.29 (3.6)	1.44 (0.0)	1.43 (0.0)		
0.8	6.12 (0.0)	6.19 (0.0)	1.28 (0.0)	1.27 (0.0)		
0.9	2.22 (0.0)	2.23 (0.0)	1.15 (0.0)	1.15 (0.0)		

on the scaling tendency of Recall in Table 1. Still, we find that the performance of RAR is significantly worse than that of STAR regardless of the parameter scale, and qualitative comparison in Figure 7 confirm that exposing AR models to bidirectional context is insufficient for image editing.

## 4.3. Ablation Studies

**Order Randomization Strategy** In Table 2, we compare order randomization strategies with a raster-scan order AR model, by sharing the model configurations to match that of STAR-B. In particular, we examine approaches that utilize the uniform spanning tree solely for inference or that adopt an order annealing strategy [44], which converges to the uniform spanning tree, based on the fact that the sample space of random permutations is larger than that of the uniform spanning tree. We find that the model trained with the random permutation cannot be improved through the traversal order of uniform spanning trees at inference. We speculate that this is because the sequence orders following prior knowledge of the images, which the uniform spanning tree structurally reflects, are very rare for random permutations; therefore, they are not frequently observed during training. Furthermore, we observe that models trained with uniform spanning trees consistently outperform models trained with random permutations and are comparable to those trained with a fixed raster-scan order, and the annealing strategy has no significant impact on overall performance. This reveals

that the sample space of the uniform spanning tree is sufficient to cover the advantage of the bidirectional context exposed by random permutations without increasing the training complexity, such as the order annealing strategy.

**Traversal Order for Completion** In Table 3, we conduct an ablation study on the efficiency of rejection sampling of spanning trees for achieving postfix completion, depending on the choice of BFS and DFS. We also examine the feasibility of the farthest root selection strategy for better acceptance compared to the random root selection strategy on both BFS and DFS. We measure the number of trials required to sample a spanning tree that satisfies the condition for postfix completion under the corresponding traversal order, for 50k random connected masks with masking ratios ranging from 0.1 to 0.9 in increments of 0.1. The maximum number of trials for each random mask is bounded at 100, and any case that cannot be obtained within this bound is considered a failure. We find that DFS requires significantly more trials than BFS and fails more frequently, whereas BFS can generally sample the spanning tree under five trials. Furthermore, the farthest root strategy further reduces the number of trials at a relatively small masking ratio. This demonstrates the validity of selecting the BFS as the default traversal strategy of the spanning tree in STAR.

#### 5. Conclusion

In this work, we propose Spanning Tree Autoregressive (STAR) modeling, which adopts BFS traversal order of uniform spanning starting from the corner of the lattice as the randomized sequence order of AR visual generation models. By adopting the traversal order of a uniform spanning tree that structurally reflects prior knowledge of the image, it achieves image editing capability through the flexibility of choice in sequence orders for image editing and sampling performance simultaneously. Notably, STAR achieves bidirectional context-sampling performance and robustness with a simple learning structure, with only minimal changes to the conventional AR visual modeling architecture. The simplicity of STAR can serve as a building block for future works on diverse extensions of AR visual modeling.

# **Spanning Tree Autoregressive Visual Generation**

# Supplementary Material

## A. Hyperparameter Configurations

Table A. Detailed hyperparameter configurations of STAR.

Hyperparameter	STAR-B	STAR-L	STAR-XL	STAR-XXL		
Depth	24	24	32	40		
Width	768	1024	1280	1480		
Feedforward Dim	3072	4096	5120	6144		
Attention Heads	16	16	16	16		
Optimizer		A	damW			
$(\beta_0, \beta_1)$		(0.	.9, 0.96)			
Weight Decay			0.03			
LR Scheduler	cosine with linear warmup					
Peak Learning Rate	4e-4					
Decay Learning Rate		1e-5				
Warmup Ratio	0.25					
Batch Size	2048					
Training Steps	250,000					
Precision	bfloat16					
Gradient Clipping	1.0					
Attention Dropout	0.1					
Feedforward Dropout	0.1					
Class Label Dropout	0.1					
CFG Scheduler	pow-cosine					
Guidance Scale	16.0	14.5	6.5	5.4		
Guidance Power	2.75	2.55	1.5	1.25		
Sampling Temperature	0.98	0.98	0.98	0.98		

# **B.** Masking Strategy for Inpainting Evaluation

We adopt a random masking strategy to quantitatively evaluate inpainting performance across various mask types, varying the masking ratio from 0.1 to 0.9 in 0.1 increments while still covering a range of general inpainting scenarios. Starting from a single random patch region, we incrementally add adjacent patches to the current mask until the given masking ratio R is reached, ensuring that both the masked and non-masked regions remain connected. Algorithm A denotes the pseudo-code for the random masking strategy.

## **Algorithm A** Random Masking Strategy for Inpainting

```
Require: lattice G := (V, E), masking ratio R
 1: repeat
         V_M \leftarrow \{v \sim V\}
 2:
         while |V_M| < R \times |V| do
 3:
            B \leftarrow \{v \in V \setminus V_M \mid \exists u \in V_M \text{ s.t. } (u, v) \in E\}
 4:
            V_M \leftarrow V_M \cup \{v_M \sim B\}
 5:
         end while
 6:
         E_M \leftarrow \{(u,v) \mid \forall u,v \in V_M \text{ s.t. } (u,v) \in E\}
 7:
         M \leftarrow (V_M, E_M)
 9: until G \setminus M is connected
```

10: **return** mask M

# C. Additional Analysis of Conditional Entropy

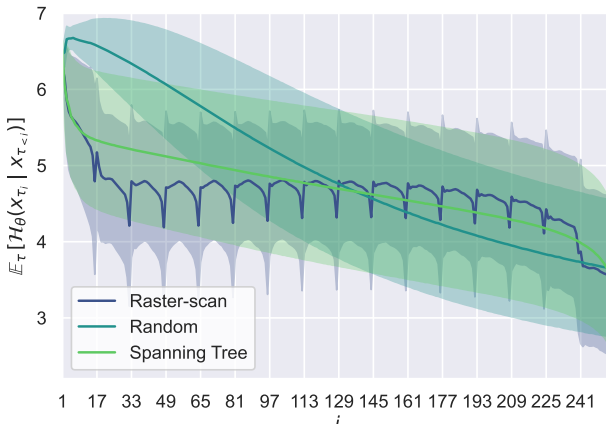


Figure A. Conditional prediction entropy according to the token position in the 1D sequence order. Sequence orders with better sampling performance tend to have a uniform scale of conditional prediction entropy across token positions in 1D sequences.

We have verified that prior knowledge observed in the image is preserved in the 2D lattice of patch token representation at Section 3.2, but it does not demonstrate the characteristic of prediction entropy according to the linearized 1D sequence order actually used in AR modeling. In this sense, we similarly compare the prediction conditional entropy of validation images according to token position in the 1D sequence for models trained under raster-scan, random permutation, and BFS traversal order of the spanning tree.

In Figure A, we observe that the conditional prediction entropy of the AR model trained on the spanning tree exhibits characteristics similar to the AR model with rasterscan order, in terms of the scale change according to the token position. Specifically, in the case of a random permutation, it shows high conditional prediction entropy at the initial token positions, but then decays quickly after half of the token positions; in the case of raster-scan and spanning tree, it is relatively constant across token positions.

Therefore, we presume that adopting sequence orders that reflect prior knowledge observed in the image corresponds to choosing sequence orders with relatively uniform conditional data entropy across token positions. Given that both cases show superior sampling performance compared to the random permutation case, we speculate that the sampling performance of AR models is related to uniformity in the conditional entropy per token across sequence order.

# D. Additional Examples of Sampled Results



Figure B. Sampled results in the class-conditional image generation on ImageNet-1k at  $256 \times 256$  (class ID: 47, chamaeleon).



Figure C. Sampled results in the class-conditional image generation on ImageNet-1k at  $256 \times 256$  (class ID: 145, king penguin).



Figure D. Sampled results in the class-conditional image generation on ImageNet-1k at  $256 \times 256$  (class ID: 207, golden retriever).



Figure E. Sampled results in the class-conditional image generation on ImageNet-1k at  $256 \times 256$  (class ID: 360, otter).



Figure F. Sampled results in the class-conditional image generation on ImageNet-1k at  $256 \times 256$  (class ID: 417, balloon).



Figure G. Sampled results in the class-conditional image generation on ImageNet-1k at  $256 \times 256$  (class ID: 950, orange).



Figure H. Sampled results in the class-conditional image generation on ImageNet-1k at  $256 \times 256$  (class ID: 972, cliff).



Figure I. Sampled results in the class-conditional image generation on ImageNet-1k at  $256 \times 256$  (class ID: 980, volcano).

# Acknowledgements

This work was supported by LG AI Research. This work was supported by the Institute of Information & Communications Technology Planning & Evaluation (IITP) grants funded by the Korea government (MSIT) (No. RS-2025-II211343, Artificial Intelligence Graduate School Program (Seoul National University)). This work was supported by the National Research Foundation of Korea (NRF) grants funded by the Korean government (MSIT) (Nos. RS-2024-00354218 and RS-2024-00353125). This work was supported by the Institute of Information & Communications Technology Planning & Evaluation (IITP) grants funded by the Korea government (MSIT) (No. RS-2025-02263598, Development of Self-Evolving Embodied AGI Platform Technology through Real-World Experience). This work was supported by an IITP grant funded by the Korean Government (MSIT) (No. RS-2024-00353131).

#### References

- [1] Fan Bao, Shen Nie, Kaiwen Xue, Yue Cao, Chongxuan Li, Hang Su, and Jun Zhu. All are worth words: A vit backbone for diffusion models. In *Proceedings of the IEEE/CVF conference on computer vision and pattern recognition*, pages 22669–22679, 2023. 1, 2, 6
- [2] Victor Besnier, Mickael Chen, David Hurych, Eduardo Valle, and Matthieu Cord. Halton scheduler for masked generative image transformer. *arXiv preprint arXiv:2503.17076*, 2025. 2, 4
- [3] Ali Borji and James Tanner. Reconciling saliency and object center-bias hypotheses in explaining free-viewing fixations. *IEEE transactions on neural networks and learning systems*, 27(6):1214–1226, 2015. 2, 4
- [4] Tom Brown, Benjamin Mann, Nick Ryder, Melanie Subbiah, Jared D Kaplan, Prafulla Dhariwal, Arvind Neelakantan, Pranav Shyam, Girish Sastry, Amanda Askell, et al. Language models are few-shot learners. Advances in neural information processing systems, 33:1877–1901, 2020.
- [5] Huiwen Chang, Han Zhang, Lu Jiang, Ce Liu, and William T Freeman. Maskgit: Masked generative image transformer. In Proceedings of the IEEE/CVF conference on computer vision and pattern recognition, pages 11315–11325, 2022. 1, 2, 5
- [6] Mark Chen, Alec Radford, Rewon Child, Jeffrey Wu, Heewoo Jun, David Luan, and Ilya Sutskever. Generative pretraining from pixels. In *International conference on machine learning*, pages 1691–1703. PMLR, 2020. 1, 2, 3
- [7] Mostafa Dehghani, Josip Djolonga, Basil Mustafa, Piotr Padlewski, Jonathan Heek, Justin Gilmer, Andreas Peter Steiner, Mathilde Caron, Robert Geirhos, Ibrahim Alabdulmohsin, et al. Scaling vision transformers to 22 billion parameters. In *International conference on machine learning*, pages 7480–7512. PMLR, 2023. 5
- [8] Jia Deng, Wei Dong, Richard Socher, Li-Jia Li, Kai Li, and Li Fei-Fei. Imagenet: A large-scale hierarchical image database. In 2009 IEEE conference on computer vision and pattern recognition, pages 248–255. Ieee, 2009. 4, 5

- [9] Prafulla Dhariwal and Alexander Nichol. Diffusion models beat gans on image synthesis. *Advances in neural information processing systems*, 34:8780–8794, 2021. 6
- [10] Alexey Dosovitskiy. An image is worth 16x16 words: Transformers for image recognition at scale. arXiv preprint arXiv:2010.11929, 2020. 5
- [11] Alaaeldin El-Nouby, Michal Klein, Shuangfei Zhai, Miguel Angel Bautista, Vaishaal Shankar, Alexander Toshev, Joshua M Susskind, and Armand Joulin. Scalable pretraining of large autoregressive image models. In Proceedings of the 41st International Conference on Machine Learning, pages 12371–12384, 2024. 1, 3
- [12] Patrick Esser, Robin Rombach, and Bjorn Ommer. Taming transformers for high-resolution image synthesis. In Proceedings of the IEEE/CVF conference on computer vision and pattern recognition, pages 12873–12883, 2021. 2, 3, 5
- [13] Shanghua Gao, Pan Zhou, Ming-Ming Cheng, and Shuicheng Yan. Masked diffusion transformer is a strong image synthesizer. In *Proceedings of the IEEE/CVF interna*tional conference on computer vision, pages 23164–23173, 2023. 6
- [14] Tom Henighan, Jared Kaplan, Mor Katz, Mark Chen, Christopher Hesse, Jacob Jackson, Heewoo Jun, Tom B Brown, Prafulla Dhariwal, Scott Gray, et al. Scaling laws for autoregressive generative modeling. *arXiv preprint arXiv:2010.14701*, 2020. 1, 2
- [15] Martin Heusel, Hubert Ramsauer, Thomas Unterthiner, Bernhard Nessler, and Sepp Hochreiter. Gans trained by a two time-scale update rule converge to a local nash equilibrium. Advances in neural information processing systems, 30, 2017. 6
- [16] Jonathan Ho and Tim Salimans. Classifier-free diffusion guidance. arXiv preprint arXiv:2207.12598, 2022. 6
- [17] Jonathan Ho, Ajay Jain, and Pieter Abbeel. Denoising diffusion probabilistic models. *Advances in neural information processing systems*, 33:6840–6851, 2020. 1, 2
- [18] Jinggang Huang and David Mumford. Statistics of natural images and models. In *Proceedings. 1999 IEEE Computer Society Conference on Computer Vision and Pattern Recog*nition (Cat. No PR00149), pages 541–547. IEEE, 1999. 2,
- [19] Jared Kaplan, Sam McCandlish, Tom Henighan, Tom B Brown, Benjamin Chess, Rewon Child, Scott Gray, Alec Radford, Jeffrey Wu, and Dario Amodei. Scaling laws for neural language models. arXiv preprint arXiv:2001.08361, 2020. 1, 2
- [20] Maciej Kilian, Varun Jampani, and Luke Zettlemoyer. Computational tradeoffs in image synthesis: Diffusion, masked-token, and next-token prediction. arXiv preprint arXiv:2405.13218, 2024. 1, 2
- [21] Tuomas Kynkäänniemi, Tero Karras, Samuli Laine, Jaakko Lehtinen, and Timo Aila. Improved precision and recall metric for assessing generative models. *Advances in neural information processing systems*, 32, 2019. 6
- [22] Doyup Lee, Chiheon Kim, Saehoon Kim, Minsu Cho, and Wook-Shin Han. Autoregressive image generation using residual quantization. In *Proceedings of the IEEE/CVF con-*

- ference on computer vision and pattern recognition, pages 11523-11532, 2022. 2
- [23] Haopeng Li, Jinyue Yang, Guoqi Li, and Huan Wang. Autoregressive image generation with randomized parallel decoding. arXiv preprint arXiv:2503.10568, 2025. 1, 2, 3, 7
- [24] Tianhong Li, Yonglong Tian, He Li, Mingyang Deng, and Kaiming He. Autoregressive image generation without vector quantization. Advances in Neural Information Processing Systems, 37:56424–56445, 2024. 6
- [25] Xuantong Liu, Shaozhe Hao, Xianbiao Qi, Tianyang Hu, Jun Wang, Rong Xiao, and Yuan Yao. Elucidating the design space of language models for image generation. arXiv preprint arXiv:2410.16257, 2024. 1, 2
- [26] Ziqi Pang, Tianyuan Zhang, Fujun Luan, Yunze Man, Hao Tan, Kai Zhang, William T Freeman, and Yu-Xiong Wang. Randar: Decoder-only autoregressive visual generation in random orders. In *Proceedings of the Computer Vision and Pattern Recognition Conference*, pages 45–55, 2025. 1, 2, 3, 6, 7
- [27] Arnaud Pannatier, Evann Courdier, and François Fleuret. σ-gpts: A new approach to autoregressive models. In *Joint European Conference on Machine Learning and Knowledge Discovery in Databases*, pages 143–159. Springer, 2024. 1, 2, 5, 6
- [28] William Peebles and Saining Xie. Scalable diffusion models with transformers. In *Proceedings of the IEEE/CVF international conference on computer vision*, pages 4195–4205, 2023. 1, 2, 6
- [29] Alec Radford, Jeffrey Wu, Rewon Child, David Luan, Dario Amodei, Ilya Sutskever, et al. Language models are unsupervised multitask learners. *OpenAI blog*, 1(8):9, 2019. 1,
- [30] Tim Salimans, Ian Goodfellow, Wojciech Zaremba, Vicki Cheung, Alec Radford, and Xi Chen. Improved techniques for training gans. Advances in neural information processing systems, 29, 2016. 6
- [31] Robert Shrock and Fa Yueh Wu. Spanningtrees on graphs and lattices in d dimensions. *Journal of Physics A: Mathematical and General*, 33(21):3881, 2000. 4
- [32] Peize Sun, Yi Jiang, Shoufa Chen, Shilong Zhang, Bingyue Peng, Ping Luo, and Zehuan Yuan. Autoregressive model beats diffusion: Llama for scalable image generation. *arXiv* preprint arXiv:2406.06525, 2024. 2, 6, 7
- [33] Gergely Szabó and András Horváth. Mitigating the bias of centered objects in common datasets. In 2022 26th International Conference on Pattern Recognition (ICPR), pages 4786–4792. IEEE, 2022. 2, 4
- [34] Christian Szegedy, Wei Liu, Yangqing Jia, Pierre Sermanet, Scott Reed, Dragomir Anguelov, Dumitru Erhan, Vincent Vanhoucke, and Andrew Rabinovich. Going deeper with convolutions. In *Proceedings of the IEEE conference on computer vision and pattern recognition*, pages 1–9, 2015.
- [35] Chameleon Team. Chameleon: Mixed-modal early-fusion foundation models. *arXiv preprint arXiv:2405.09818*, 2024. 1, 2
- [36] Keyu Tian, Yi Jiang, Zehuan Yuan, Bingyue Peng, and Liwei Wang. Visual autoregressive modeling: Scalable image

- generation via next-scale prediction. *Advances in neural information processing systems*, 37:84839–84865, 2024. 2, 6, 7
- [37] Hugo Touvron, Thibaut Lavril, Gautier Izacard, Xavier Martinet, Marie-Anne Lachaux, Timothée Lacroix, Baptiste Rozière, Naman Goyal, Eric Hambro, Faisal Azhar, et al. Llama: Open and efficient foundation language models. arXiv preprint arXiv:2302.13971, 2023. 1, 2
- [38] Aäron Van Den Oord, Nal Kalchbrenner, and Koray Kavukcuoglu. Pixel recurrent neural networks. In *Interna*tional conference on machine learning, pages 1747–1756. PMLR, 2016. 1, 2
- [39] Aaron Van Den Oord, Oriol Vinyals, et al. Neural discrete representation learning. Advances in neural information processing systems, 30, 2017. 1, 2
- [40] Xi Wang, Nicolas Dufour, Nefeli Andreou, Marie-Paule Cani, Victoria Fernández Abrevaya, David Picard, and Vicky Kalogeiton. Analysis of classifier-free guidance weight schedulers. Transactions on Machine Learning Research Journal, 2024. 6
- [41] David Bruce Wilson. Generating random spanning trees more quickly than the cover time. In *Proceedings of the twenty-eighth annual ACM symposium on Theory of computing*, pages 296–303, 1996. 4, 6
- [42] Zhilin Yang, Zihang Dai, Yiming Yang, Jaime Carbonell, Russ R Salakhutdinov, and Quoc V Le. Xlnet: Generalized autoregressive pretraining for language understanding. Advances in neural information processing systems, 32, 2019. 1, 2
- [43] Jiahui Yu, Xin Li, Jing Yu Koh, Han Zhang, Ruoming Pang, James Qin, Alexander Ku, Yuanzhong Xu, Jason Baldridge, and Yonghui Wu. Vector-quantized image modeling with improved vqgan. arXiv preprint arXiv:2110.04627, 2021. 2
- [44] Qihang Yu, Ju He, Xueqing Deng, Xiaohui Shen, and Liang-Chieh Chen. Randomized autoregressive visual generation. In *Proceedings of the IEEE/CVF International Conference on Computer Vision*, pages 18431–18441, 2025. 1, 2, 3, 5, 6, 7, 8